





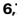











On-surface synthesis of ballbot-type N-heterocyclic carbene polymers

Received: 25 January 2022

Accepted: 26 July 2023

Published online: 28 August 2023


 Check for updates

Jindong Ren ^{1,2,3}, Maximilian Koy ⁴, Helena Osthues ⁵,
Bertram Schulze Lammers^{2,3}, Christian Gutheil⁴, Marvin Nyenhuis⁵,
Qi Zheng ^{6,7}, Yao Xiao^{6,7}, Li Huang ^{6,7}, Arne Nalop⁴, Qing Dai ¹,
Hong-Jun Gao ^{6,7} , Harry Mönig ^{2,3} , Nikos L. Doltsinis ⁵ ,
Harald Fuchs ^{2,3}  & Frank Glorius ⁴ 

N-Heterocyclic carbenes (NHCs) are established ligands for metal complexes and surfaces. Here we go beyond monomeric NHCs and report on the synthesis of NHC polymers on gold surfaces, consisting of ballbot-type repeating units bound to single Au adatoms. We designed, synthesized and deposited precursors containing different halogens on gold surfaces under ultrahigh vacuum. Conformational, electronic and charge transport properties were assessed by combining low-temperature scanning tunneling microscopy, non-contact atomic force microscopy, X-ray photoelectron spectroscopy, first-principles calculations and reactive force field simulations. The confirmed ballbot-type nature of the NHCs explains the high surface mobility of the incommensurate NHC polymers, which is prerequisite for their desired spatial alignment. The delicate balance between mobility and polymerization rate allows essential parameters for controlling polymer directionality to be derived. These polymers open up new opportunities in the fields of nanoelectronics, surface functionalization and catalysis.

Surface modification by organic molecules is an attractive technique that allows important properties to be tuned for catalysis and materials science, such as selectivity of catalytic reactions or electronics^{1,2}. Controlling the supramolecular assembly of organic molecules on metal surfaces is often challenging because it is driven by complex intermolecular interactions³. Covalent on-surface polymerization^{4,5}, which is a rapidly developing field, promises to overcome some of the limitations of self-assembly to obtain well-controllable surface functionalization structures with potential applications in catalysis, molecular electronics and gas sensing⁶. Additionally, surface-bound

molecules can show polymerization modes that are otherwise elusive, paving the way to novel chemical species⁷. NHCs have been increasingly applied as highly attractive molecular modifiers and anchors for various surfaces because of the formation of stable bonds and their strong electron donation and unique steric properties^{8–10}. Applications of NHC-modified surfaces in the fields of catalysis and materials science have been reported^{8–16}. Detailed mechanistic studies have revealed various binding modes and a potential explanation for the high mobility of some NHCs: they can—depending on the substitution pattern of the nitrogen atoms—extract single atoms from the surface and display a

¹CAS Key Laboratory of Nanophotonic Materials and Devices, CAS Key Laboratory of Standardization and Measurement for Nanotechnology, National Center for Nanoscience and Technology, Beijing, PR China. ²Physikalisches Institut, Westfälische Wilhelms-Universität, Münster, Germany. ³Center for Nanotechnology, Münster, Germany. ⁴Organisch-Chemisches Institut, Westfälische Wilhelms-Universität, Münster, Germany. ⁵Institute for Solid State Theory and Center for Multiscale Theory and Computation, Westfälische Wilhelms-Universität, Münster, Germany. ⁶Beijing National Center for Condensed Matter Physics and Institute of Physics, Chinese Academy of Sciences, Beijing, PR China. ⁷University of Chinese Academy of Sciences, Chinese Academy of Sciences, Beijing, PR China.  e-mail: hjgao@iphy.ac.cn; harry.moenig@uni-muenster.de; nikos.doltsinis@uni-muenster.de; fuchsh@uni-muenster.de; glorius@uni-muenster.de

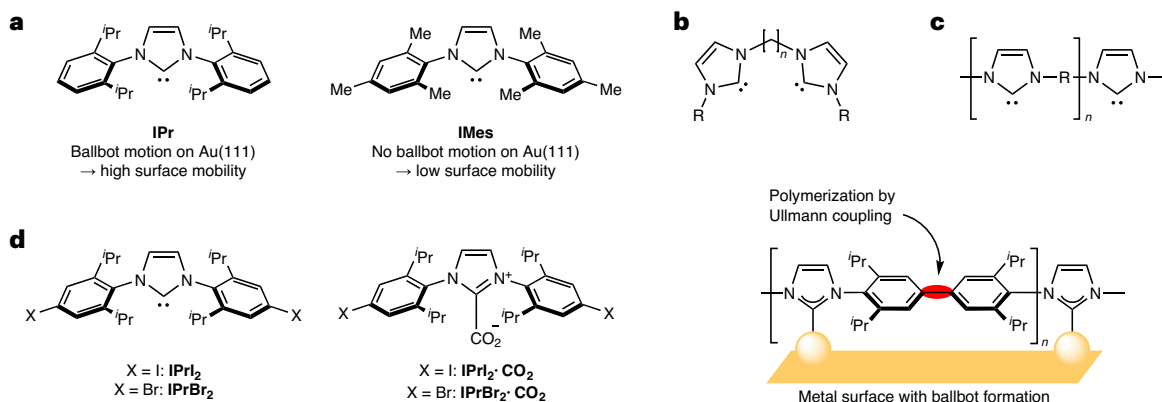


Fig. 1 General aspects of NHCs on surfaces. **a**, Surface mobility is dependant on NHC structure. **b**, Bidentate NHC ligand established in catalysis. **c**, Poly-NHC species with the NHCs as the repetition unit. **d**, Monomeric NHCs from this study

(left), their zwitterionic precursors (middle) and the repetition unit of the polymeric structure (right). **IPr**, 1,3-bis(2,6-diisopropylphenyl)imidazol-2-ylidene; **IMes**, 1,3-dimesitylimidazol-2-ylidene.

ballbot-type¹⁷ motion (Fig. 1a, Supplementary Fig. I-1). Simultaneously, monomeric NHCs with defined side groups act as efficient molecular modifiers for heterogeneous catalysis with metal surfaces and have promoted significant levels of stability, reactivity and enantioselectivity^{18–20}. Indeed, the catalytic efficiency should be further improved on repeatedly ordered NHC supramolecular structures, because the reactants will be forced to slide along certain directions²¹. Furthermore, the preorganization effect originating from ordered structures could also provide a platform for building unprecedented composites with unique structures and properties⁶. Although several supramolecular architectures have been realized by self-assembly of individual NHCs²², substantial stability including increased tensile strength is required under harsh conditions, such as high voltage and current²³ or high temperature²⁴.

To the best of our knowledge, direct imaging of covalently linked polymeric NHC species on a surface has not yet been reported. This is probably due to the high polymer weight, which makes direct evaporation extremely challenging. Nevertheless, the beneficial effect of multidentate NHC ligands is well known in homogeneous catalysis²⁵ and their potential for the modification of surfaces^{24,26} has recently been demonstrated (Fig. 1b). We believe that polymers using simple NHCs⁹ as the repeating units would show unprecedented properties and simultaneously open new gateways for surface functionalization (Fig. 1c). Ullmann coupling²⁷ mediated by metal catalysts has—owing to its reliability and controllability—been recognized as a powerful method to form various covalently bound nanostructures^{28,29}. Reaction conditions including molecular precursors³⁰, annealing temperature³¹ and substrate species³² have been widely studied using scanning probe microscopy (SPM) and X-ray photoelectron spectroscopy (XPS)³³. Thus, surface-assisted reactions using such well-established methods allow control of ballbot-type polymeric growth processes and enable research on novel physicochemical properties resulting from this type of surface functionalization.

Here, we achieve in-situ formation of robust, covalently connected NHC polymers by Ullmann coupling under ultrahigh vacuum (UHV) conditions and highly defined single crystalline gold surfaces. We selected bis-halogenated NHCs **IPrI₂** and **IPrBr₂** (Fig. 1d) to synthesize linear polymers via on-surface polymerization. Deeper insight into the NHC polymerization process is gained by low-temperature scanning tunneling microscopy (STM), non-contact atomic force microscopy (nc-AFM), XPS, density functional theory (DFT) and reactive force field (ReaxFF) calculations. The nc-AFM experiments were performed with two different types of atomically defined probe-tip terminations (CO- (ref. 34) and O-terminated³⁵ Cu (CuOx) tips) to achieve ultrahigh

resolution, uncovering conformational information on the involved NHC structures. The ballbot-like nature¹⁷ of selected NHCs was quantitatively characterized both experimentally and theoretically³⁶. Such unique adatom-promoted NHC polymers not only show high surface mobility, but also form incommensurate structures on the surface. Furthermore, to build richer varieties of NHC-based supramolecular architectures, different halogen precursors and growth conditions are explored to control the polymer directionality. Well-ordered polymers with tunable directional alignments can be prepared on Au(100) substrates and explained by the thermodynamical factors in terms of precursor mobility and activation barriers.

Results and discussion

To reveal the surface binding mode of **IPrI₂** monomers, nc-AFM experiments as well as DFT calculations were performed. The bright centre in the nc-AFM contrast can be attributed to the upstanding NHC ring with two up-facing H atoms³⁷, whereas the four surrounding darker contrast features correspond to the topographically lower lying *iPr* groups (Fig. 2a–c). DFT geometry optimizations show strong covalent bonding between the carbene and a gold surface atom which can easily be extracted from the surface (Supplementary Fig. II-3) to form the so-called ballbot species¹⁷ (Fig. 2d). The remaining vacancy is refilled with an atom from the subjacent gold layer. The exact position of the NHC–Au adatom complex with respect to the underlying gold lattice is observed by constant-height nc-AFM (Fig. 2a,b). The surface Au lattice grid was determined from the atomically resolved images of the Au(111) surface in Supplementary Fig. II-2. For a ballbot-type complex with the Au adatom occupying a face-centred cubic (fcc) site³⁸, the simulated AFM image (Fig. 2c) based on the DFT optimized geometry (Supplementary Fig. II-2b) fits well to our experimental observation (Fig. 2b). The slightly tilted geometry of the NHC was inferred from the contrast difference of the *iPr* groups.

The extraction of a gold atom, that is, ballbot formation, agrees with height measurements of the highest H atom with respect to the surface. Figure 2d,e displays the detected $\Delta f(z)$ curves on an isolated **IPrI₂** monomer and the Au(111) surface with a CO tip where the height difference is estimated from the minima³⁹. This is further analysed by comparison with theoretical simulations considering possible effects due to differences in the chemical interactions with the probe tip on the different sites. The difference of 6.0 Å for the tilted **IPrI₂** monomer is in line with 6.0 Å from simulated spectra (Supplementary Fig. II-6) for the ballbot configuration, whereas 5.0 Å was found for the non-ballbot configuration. This result is strongly underpinned by a direct comparison of $\Delta f(z)$ spectra recorded on ballbot and non-ballbot NHCs,

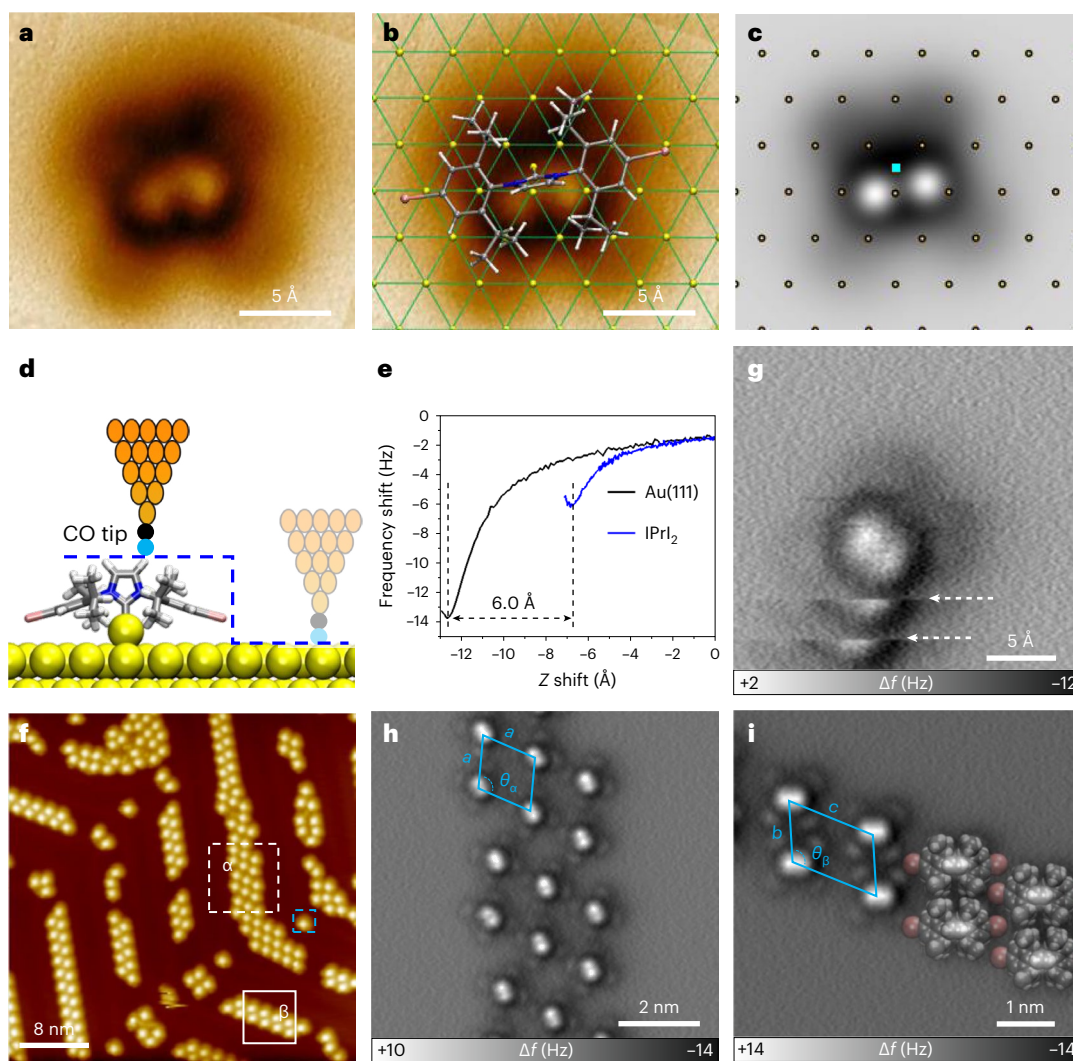


Fig. 2 | Self-assembly of IPr₁₂ on Au(111). **a, b**, High-resolution constant-height nc-AFM image (**a**) with experimentally determined underlying gold lattice (green; **b**). The DFT-optimized geometry of ballbot-type IPr₁₂ in the fcc position is superimposed in **b**. This tilted orientation of the molecule is only 0.08 eV higher in energy than the upright position. **c**, Simulated AFM image based on the DFT-optimized structure and a previously reported probe particle model⁵⁹. The top-layer gold atoms are indicated by yellow dots; the adatom position by a light blue square. **d**, Side-view of a DFT-optimized structure demonstrating the upright binding mode of the ballbot species. Pink sticks represent the iodine atoms. **e**, The frequency-displacement curves obtained by nc-AFM as shown in **d**.

f, STM topography of IPr₁₂ shows preferred adsorption at fcc regions. **g**, Constant-height nc-AFM image of an individual monomer (light blue dashed square in **f**) shows several lateral jumps due to high surface mobility, two white dashed arrows highlight the jump positions. The iodine atoms are located even lower (**d**) and can therefore not be imaged. **h, i**, An nc-AFM close-up from the areas indicated as white dashed (**h**) and solid (**i**) squares in **f**. The DFT-optimized self-assembly is superimposed on the observed structure in **i**. $a = 1.3$ nm, $\theta_a = 108^\circ$; $b = 1.1$ nm, $c = 1.5$ nm, $\theta_b = 120^\circ$. All SPM data were acquired at 4.5 K. Data in **a** and **e** were acquired with a CO-tip, in **f–i** with a CuOx tip.

which have been co-deposited on the same surface (Supplementary Figs. II-8 and II-11 and corresponding discussion). Further support for the ballbot-type configuration is provided by analysing the nc-AFM contrast in more detail. This is based on the fact that the presence of the extracted Au atom below the NHC allows the ⁱPr groups to relax toward the surface. This, in turn, leads to a considerably weaker contrast with respect to the up-facing H atoms at the NHC unit, which is in full agreement with experimental and simulated contrasts. Contrastingly, for a non-ballbot type configuration, the ⁱPr groups are pushed up by steric repulsion due to the closer substrate leading to considerably more pronounced ⁱPr contrast signatures. Moreover, the relaxation of the ⁱPr groups goes along with a distinct rotation of the ⁱPr groups moving their uppermost atoms away from the molecular centre, which is in excellent agreement with experimental and simulated distances (Supplementary Fig. II-9 and a more detailed discussion in Supplementary

Section 2.3). The IPr₁₂ molecules show high mobility at 4.5 K (Fig. 2g). During the scanning process, several lateral hopping movements of the monomer can be observed (white arrows in Fig. 2g). We also quantitatively determined the lateral force to move an NHC with the nc-AFM tip (Supplementary Fig. II-10): an attractive lateral shear force threshold of -354 pN. Previous reports have shown that the forces measured in strong chemical bonds are of the order of nanonewtons⁴⁰ and the force required to move an adatom on a metal surface is usually tens to hundreds of piconewtons⁴¹. Thus, the high mobility at temperatures as low as 4.5 K, the measurements of molecular height, the contrast and the lateral force in the nc-AFM experiment all, conclusively support the theoretical prediction of a ballbot-type species.

Figure 2f shows a large-scale STM image of the Au(111) surface with sub-monolayer coverage^{42–47} of IPr₁₂ molecules. Self-assembled islands with two dominating structures, α and β phases, are identified. Figure 2h

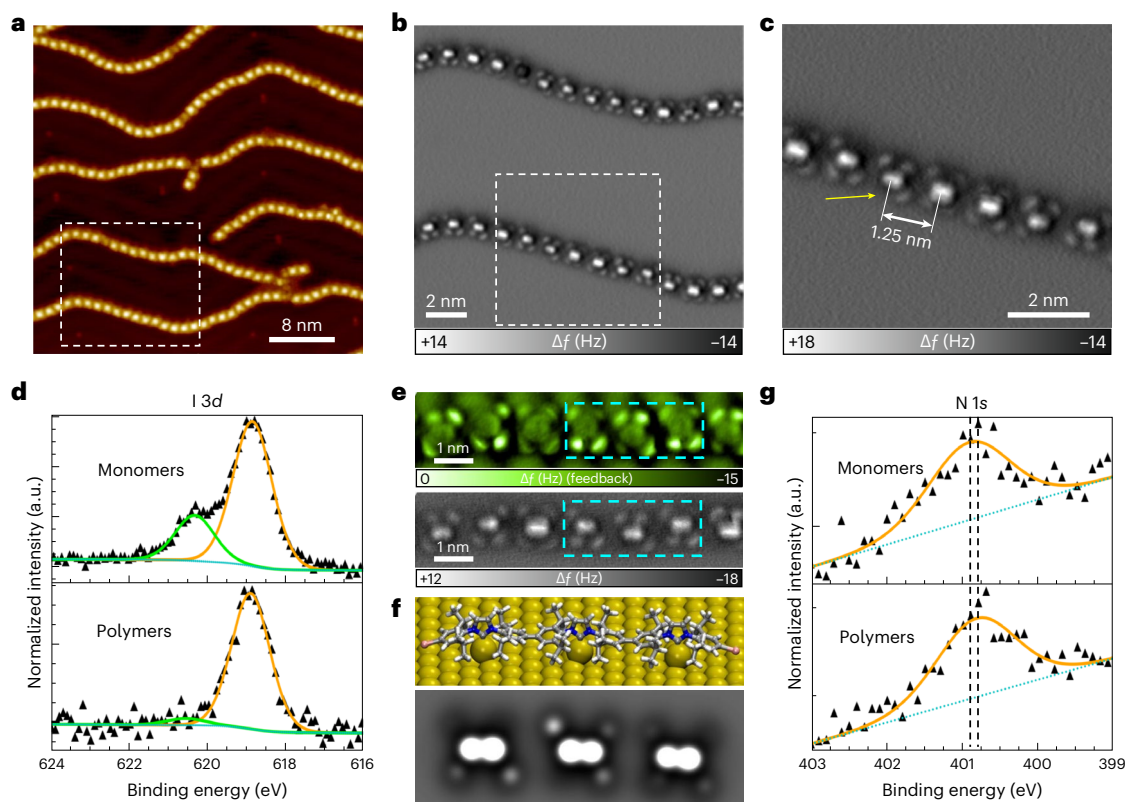


Fig. 3 | Polymerization of IPrI_2 on Au(111). **a**, Large-scale STM topography of NHC polymers after heat-induced polymerization reaction at 400 K. **b,c**, Constant-height nc-AFM of the area indicated by the white square in **a** and **b**. **d**, XPS spectra of I 3d of IPrI_2 on Au(111) acquired after RT deposition (top) and subsequent annealing to 400 K (bottom). **e**, Data (nc-AFM) with STM-feedback on (top) and off (constant-height, bottom) modes of the same polymer. **f**, Simulated

nc-AFM image (bottom) based on the DFT-optimized structure (top) and a previous probe particle model⁵⁹. **g**, N 1s XPS peaks of NHC monomers (top) and polymers (bottom), show a shift from 400.91 ± 0.04 eV to 400.82 ± 0.03 eV after annealing. All SPM data were acquired at 4.5 K. Data in **a–c** and **e** were acquired by a CuOx tip termination. Raw data are represented by black triangles while solid lines show fits with a Gaussian line shape and linear background in **d** and **g**.

shows a constant-height nc-AFM image of the α phase revealing an equal distance of $a = 1.30 \pm 0.02$ nm. Accordingly, Fig. 2i shows the data from phase β where the indicated unit cell is given by $b = 1.20 \pm 0.02$ nm and $c = 1.50 \pm 0.03$ nm. To build covalent connections between IPrI_2 monomers, we annealed the sample to 400 K for 30 min. Dispersive long chains are found, which are laterally confined by the herringbone reconstruction of the Au(111) substrate (Fig. 3a,b). Figure 3c displays an nc-AFM image with increased resolution obtained from the area of the white square in Fig. 3b. The different repeat units are linearly aligned at a distance of 1.25 ± 0.05 nm, which coincides well with the DFT-optimized distance of 1.19 ± 0.01 nm (Fig. 3f) and 1.20 ± 0.01 nm from geometry optimizations of polymers with the ReaxFF calculations (Supplementary Fig. IV-3). Thus, metal–organic complexes with incorporated Au atoms can be excluded because of their larger inter-unit distance and nonlinear shape (Supplementary Fig. IV-1).

The formation of new C–C bonds is further validated by the chemical state of the I 3d_{5/2} and C 1s core level spectra⁴⁸ from XPS measurements, which agree well with previous studies^{49–51}. We found two chemically distinct iodine components in the I 3d_{5/2} peaks (Fig. 3d). The component with the lower binding energy (618.9 eV) corresponds to chemisorbed iodine on the gold substrate, while the one with the higher binding energy (620.2 eV) corresponds to the C–I bond⁵¹. It is known that on Au(111) partial dehalogenation can occur at room temperature, which is why both components can be detected even before the thermal treatment⁴⁹. The disappearance of the latter component after thermal treatment implies C–I bond dissociation in IPrI_2 precursors. Chemisorbed iodine can be located in the STM data as nucleated along the polymers (Supplementary Fig. IV-4). At the same time, the C

1s core level spectrum shows a slight change in the overall peak shape, which we found to be in agreement with the formation of C–C bonds between phenyl groups (Supplementary Fig. IV-6).

To further characterize the conformation of the newly formed polymers, we recorded nc-AFM images with an even higher resolution (Fig. 3e). All four isopropyl groups in IPrI_2 monomers are clearly visible as dim lobes, whereas only three lobes are seen in some polymerized units. The occasional absence of a lobe (for example, the yellow arrow in Fig. 3c) is unlikely to be due to the removal of an isopropyl group during annealing and should be attributed to a stronger adsorption of these units making them invisible in a constant-height nc-AFM measurement owing to the related larger distance to the tip. Figure 3e compares one such nc-AFM image (lower panel) with one recorded under STM-feedback (upper panel). The latter provides some height modulation of the tip trajectory during scanning allowing visualization of lower intramolecular units. Here, the previously missing lobes in the constant-height measurement can always be clearly located. Therefore, the invisibility of specific ⁱPr groups in the constant-height nc-AFM images can be assigned to side group distortions. From DFT optimizations for monomers as well as polymers, we find multiple stable orientations for the ⁱPr groups and hence varying heights of the side groups resulting in intensity differences in the calculated AFM images (Fig. 3f and Supplementary Fig. VI-5). Furthermore, in most cases, we find a correlation between this side group distortion and a slight tilt angle of the upward-facing hydrogen atoms of the NHC units where a lower lying ⁱPr group goes along with a slightly more pronounced contrast of the opposite H atom at the NHC unit (Fig. 3e, lower panel).

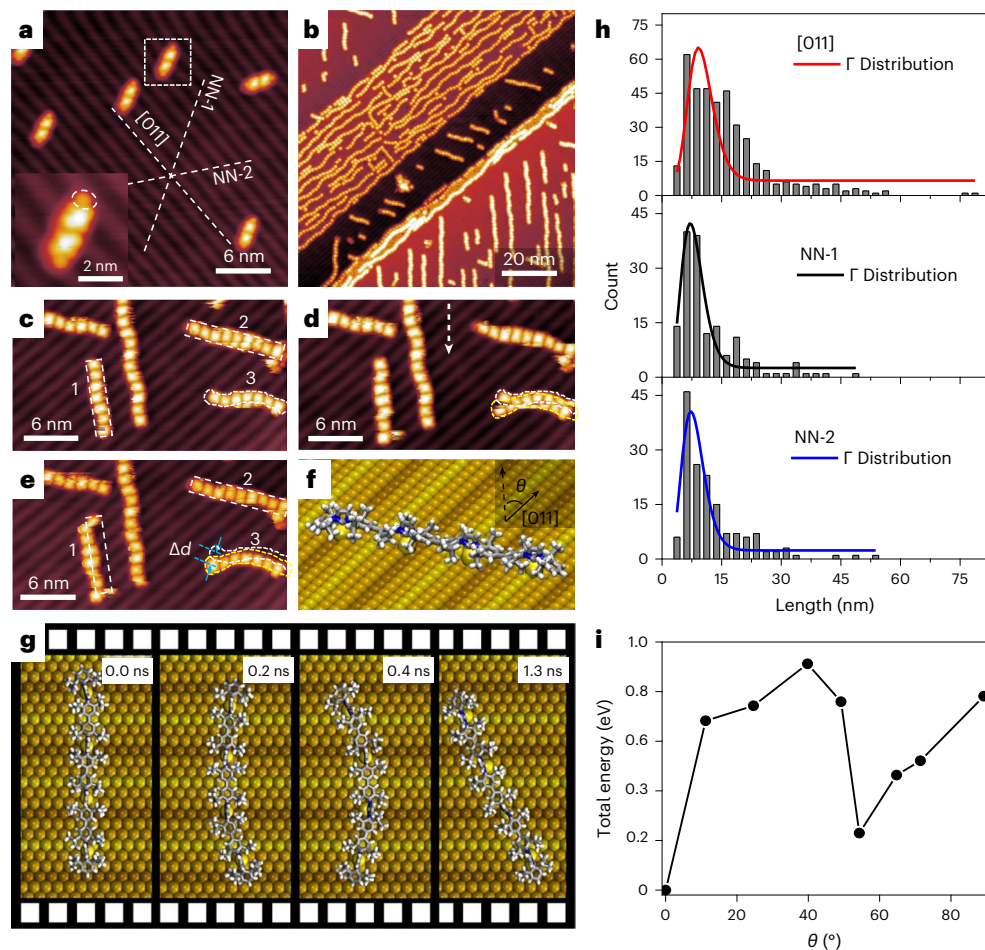


Fig. 4 | Polymers acquired from IPrI_2 molecules and their mobility and orientation on Au(100). **a**, The Ullmann reaction occurs when IPrI_2 molecules were deposited on Au(100) surface hold at 300 K. All dimers were aligned along the indicated three nearest-neighbor directions with 60° intervals. Inset: zoom-in STM topography of the white dashed square. The iodine atoms are visible at the dimer terminations (indicated by the white ellipse). **b**, Large-scale STM image indicating that IPrI_2 -based polymers are all along three orientations. **c–e**, Subsequent STM images of fixed area. The scanning direction (from top to bottom), is indicated by a white dashed arrow in **d**. A lateral displacement (Δd) of -1.4 nm was found at the left terminus of polymer ‘3’, see **e**. **f**, Side view of ballbot

NHC polymer on Au(100). **g**, Snapshots from a ReaxFF simulation of a polymer on Au(100). The different height of Au atoms in the surface reconstruction is indicated by different colors. **h**, Distribution of the polymer length from a sample similar to **b**, mean values of $L_{[011]} = 10.2$ nm, $L_{\text{NN-1}} = 8.1$ nm; $L_{\text{NN-2}} = 8.2$ nm. **i**, A total of 630 initial geometries of a 7-mer ballbot on reconstructed Au(100) were generated, relaxed and optimized using ReaxFF. The lowest total energies (in -10° increments) of the optimized geometries are plotted against the rotational angle (θ is indicated in **f**) on the surface, where 0° corresponds to an alignment with the [011] direction. All STM images were acquired at 78 K.

Up to now, we have shown the in-situ formation of covalently linked NHC polymers. Such robust connected units can supply defined catalytic sites and higher unit weight, hence making them applicable even under harsh environment. Indeed, NHCs activate otherwise inert metal systems by very strong electron donation, that is activating as a strong donor ligand for catalytic metal surfaces^{10,16}. To study the electron donation of NHC polymers, we analyzed the electron density of aromatic nitrogen substituents by XPS measurements and DFT calculations in Supplementary Figs. IV-9 and IV-7. The calculations predict an N 1s peak shift of -0.11 eV due to the removal of iodine and subsequent C–C bond formation, which agrees well with the measured shift of -0.09 ± 0.05 eV after polymerization (Fig. 3g). By evaluation of partial charges within the molecule and in the gold surface, a decreased electron donation from the molecule to the surface is found after dimerization (Supplementary Table IV-1, Supplementary Fig. IV-11–12), hinting at a decreased surface dipole and an increased work function. In fact, the calculated work function (Supplementary Fig. IV-10) increases from 4.34 eV to 4.45 eV at a coverage of 2×10^{13} molecules per cm^2 . Comparison with the corresponding NHC without iodine

(known as IPr)⁵² reveals that the work function is indeed lowered by the iodine termination and that the increase during polymerization is due to the detachment of iodine. Therefore, polymerized IPrI_2 is expected to yield a similar work function as IPr at a comparable coverage and is still in the range typical of NHCs (ref. 53).

Apart from applications of spatially periodic structures in catalysis, tuning polymer arrangements is important to construct novel NHC-functionalized electrodes and nanoelectronic devices (Supplementary Fig. V-7)⁵⁴. Therefore, controlling the polymer direction on metal surfaces was our next focus. However, the Au(111) surface is not suitable to align polymers because of the absence of a one-dimensional confinement. For example, further increasing coverage gives rise to many disordered NHC polymers in Supplementary Fig. IV-2g, with a maximum length of 100 nm for a linear polymer. For this reason, we employed the commonly used Au(100) surface, because of its straight and uniform reconstructed ridges⁵⁵.

Covalently linked dimers were discerned when depositing IPrI_2 molecules on the Au(100) surface at 300 K. Accordingly, the onset temperature for the deiodination of IPrI_2 should be less than 300 K.

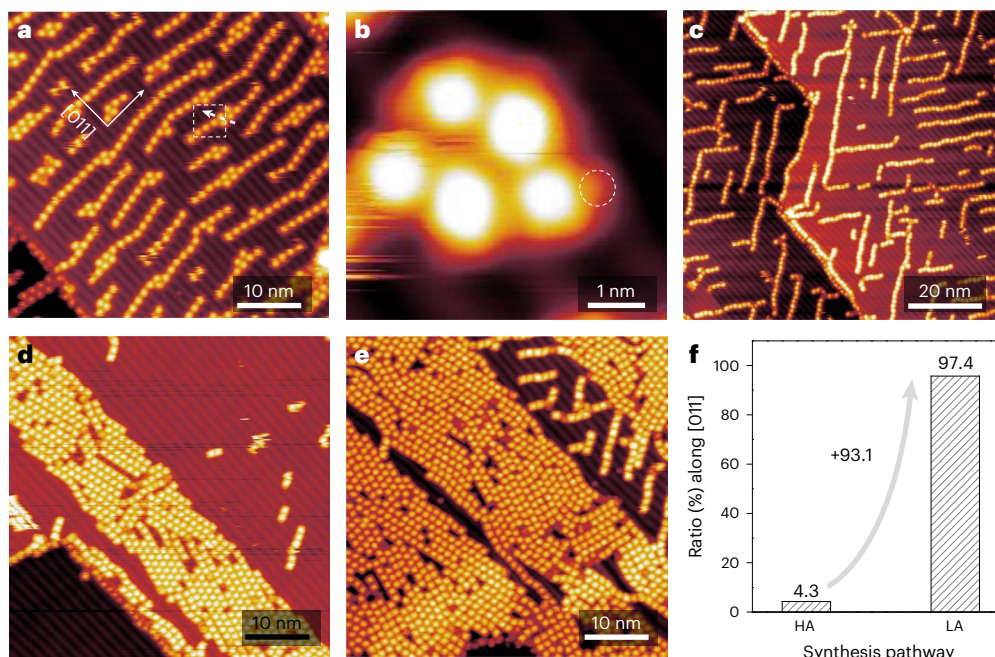


Fig. 5 | Selective formation of ordered NHC polymers on Au(100). **a**, Self-assembled IPrBr_2 monomers on Au(100) surface. **b**, The Br atoms are visible at each unit after lateral manipulation (parameters: $V = -0.03$ V; $I = -5$ nA) along the indicated direction. **c**, Quick heating to 475 K and then keeping the sample for 20 min. The NHC polymers are mainly distributed along NN-1 and NN-2

orientations. **d**, Annealing the $\text{IPrBr}_2/\text{Au}(100)$ at 375 K for 1 hour. **e**, Further depositing molecules on **d** sample and annealing at 375 K for 1 hour. **f**, Ratio of NHC polymer along [011] increases from 4.3% to 97.4% in **c** ('HA' corresponds to high annealing temperature at 475 K) and **d** ('LA' corresponds to low annealing temperature at 375 K) cases. All STM images were acquired at 78 K.

As for each dimer, the newly formed C–C bond is identified via both the uniform interval distance of 1.25 ± 0.02 nm and tip-induced rotation (Supplementary Fig. V-3). The directions of all dimers are found along the nearest-neighbor (NN) directions ([011], NN-1 and NN-2; Fig. 4a). After placing the sample at 300 K for 20 hours or annealing the sample to 400 K for 10 min, the dispersed dimers aggregated and generated longer straight chains on the surface (Fig. 4b). In fact, such a room-temperature polymerization pathway indicates a high mobility of the NHC dimers or chains on the surface.

We also studied the binding mode and surface mobility of the NHC polymers by STM measurements, DFT calculations and molecular dynamics (MD) simulations. NHC chains, originating from ballbot-type monomers, are able to move easily on the extracted gold atoms. Both twist and lateral movement of the NHC polymers marked as '1', '2' and '3' are seen at 78 K in Fig. 4c–e. This is confirmed by ReaxFF MD simulations of ballbot-type 4-mers on Au(100) (Fig. 4f,g). The ballbot formation mechanism on the Au(100) reconstructed surface considered here apparently differs from that previously observed on the Au(110) (2×1) reconstruction⁵⁶, leading to surface atomic defects followed by a (3×1) added row reconstruction. Rather, on a reconstructed Au(100) surface, due to its shallow atomic surface corrugation (Supplementary Fig. VIII-2), ballbot formation is expected to be similar to that on a Au(111) surface, for which NHC-induced surface defects are healed spontaneously by atoms originating of the second atomic layer¹⁷.

Figure 4b illustrates that the NHC polymers are well aligned along the NN directions. Due to both kinetics and thermodynamics, the synthetic process of polymers always produces chains with different orientations and lengths. Figure 4h shows the length distributions of the polymers along the NN directions. For all orientated polymers, the length distribution can be fitted well by a gamma distribution, thus supporting a random process during NHC polymer formation⁵⁷. Furthermore, the absence of oscillations in the distribution of the polymer length in Supplementary Fig. V-5 show that the polymer is incommensurate⁵⁸. To gain a better understanding of the intrinsic

mechanism regarding the three polymer alignments, the energies of differently oriented 7-mers on Au(100) were calculated. The lowest energy was found for the orientation along the [011] direction (Fig. 4i), which coincides well with the experiment and previous literature⁵⁵. A metastable orientation is seen for a rotational angle around 60° , which because of symmetry is equivalent to -60° , that is, the NN-1 and NN-2 directions.

Unique alignment of NHC polymers is critical when employing them as active components in the areas of catalysis and surface science. To obtain ordered polymers, monomeric self-assembly has to be faster than the polymerization reaction. We therefore also synthesized IPrBr_2 (Supplementary Fig. I-1) to effectively tune the direction of the NHC polymers as it is well known that C–Br cleaves at higher temperature than C–I³⁰.

Figure 5a shows an STM topography of the Au(100) surface covered with a submonolayer of IPrBr_2 . The highly ordered chains are all perpendicular to the [011] direction with a distance between two monomers of 1.58 ± 0.07 nm. We compared two different annealing protocols with regards to the polymer alignment they produce. Firstly, we heated the surface to 475 K at a rate of -1.0 K s^{-1} and held it at 475 K for 20 min (Fig. 5c). The inter-unit distance reduces to 1.26 ± 0.05 nm. Remarkably, the polymer orientations after such rapid high temperature annealing are the NN-1 and NN-2 directions, which are among the three NN preferred directions of IPrI_2 -based polymers (Fig. 4). However, in the second protocol, heating the self-assembled sample to 375 K and keeping it there for 1 hour generated unidirectional polymers along the [011] direction (Fig. 5d). At such a relatively low annealing temperature, the high mobility of IPrBr_2 monomers promotes molecular migration and aligns short intermediate polymer units.

By using the same method, further increasing the molecular coverage leads to more ordered NHC polymers on the Au(100) surface. Figure 5e is intentionally prepared at coverage of 0.87 monolayer so that the Au(100) uniformly reconstructed ridges can be recognized. Under our current annealing conditions, the majority of NHC polymers

are found along [011], but occasionally directions along NN-1 and NN-2 are also identified. Notably, the NHC polymer direction is clearly dependent on the annealing temperature, with statistical results summarized in Fig. 5f. The proportions of the polymer direction along [011] increased from 4.3% to 97.4% in Fig. 5c,d. These remarkable results display a direct proof of temperature-controlled polymer alignment.

To explain the general mechanism of temperature-dependent ballbot-type polymer alignment, the different processes during polymerization have to be considered³³. For **IPrI₂** precursors, the temperature threshold of the Ullmann reaction is low. Therefore, dehalogenation and polymerization can occur directly after deposition at 300 K (Fig. 4a). The **IPrBr₂** precursors with higher activation barrier for dehalogenation, on the other hand, first assemble in chains orthogonal to the reconstruction stripes. From this initial arrangement, two neighboring molecules only need to slightly migrate along their preferred [011] direction (Supplementary Fig. V-1) to form dimers along the NN-1 or NN-2 directions. With increasing chain length, the polymers become less mobile and hence might not be able to align in the preferred orientation parallel to the reconstruction stripes. The high activation barrier of **IPrBr₂** allows for controlled annealing. At low annealing temperatures, the slow Ullmann reaction allows for enough time for the ballbot-type NHC precursors to align along the lowest energy orientation, that is [011] direction, before long immobile polymers are formed.

Conclusions

In this study, the on-surface synthesis of covalently linked ballbot-type NHC polymers has been achieved. Their binding mode, steric as well as electronic properties and surface alignment have been studied by a combined approach of STM, nc-AFM and XPS analysis together with DFT and ReaxFF calculations allowing a comprehensive characterization of the obtained polymer species. The initial dimers and subsequent ballbot-type polymers on Au(100) align along three directions with 60° intervals as prescribed by symmetry. Statistical analysis of polymer abundance and length in these directions reveals a preferential orientation along [011], which coincides well with our theoretical lowest energy predictions. We have shown that polymer orientation can be controlled by the mobility and reactivity of the precursors. For instance, using **IPrBr₂** as precursor with mild annealing temperatures allows polymers to align before they become too long and immobile, since C–Br cleavage has a higher activation barrier than C–I cleavage. The in-depth knowledge gained from our studies will be useful for the fabrication of other novel robust carbene-based supramolecular structures and nanomaterials as well as for the enhancement of NHC-based catalytic surfaces.

Online content

Any methods, additional references, Nature Portfolio reporting summaries, source data, extended data, supplementary information, acknowledgements, peer review information; details of author contributions and competing interests; and statements of data and code availability are available at <https://doi.org/10.1038/s41557-023-01310-1>.

References

- Schoenbaum, C. A., Schwartz, D. K. & Medlin, J. W. Controlling the surface environment of heterogeneous catalysts using self-assembled monolayers. *Acc. Chem. Res.* **47**, 1438–1445 (2014).
- Mallat, T., Orglmeister, E. & Baiker, A. Asymmetric catalysis at chiral metal surfaces. *Chem. Rev.* **107**, 4863–4890 (2007).
- Love, J. C., Estroff, L. A., Kriebel, J. K., Nuzzo, R. G. & Whitesides, G. M. Self-assembled monolayers of thiolates on metals as a form of nanotechnology. *Chem. Rev.* **105**, 1103–1169 (2005).
- Judd, C. J. et al. Structural characterisation of molecular conformation and the incorporation of adatoms in an on-surface Ullmann-type reaction. *Commun. Chem.* **3**, 166 (2020).
- Grossmann, L. et al. Evolution of adsorption heights in the on-surface synthesis and decoupling of covalent organic networks on Ag(111) by normal-incidence X-ray standing wave. *Nanoscale Horiz.* **7**, 51–62 (2022).
- Grill, L. & Hecht, S. Covalent on-surface polymerization. *Nat. Chem.* **12**, 115–130 (2020).
- Ruffieux, P. et al. On-surface synthesis of graphene nanoribbons with zigzag edge topology. *Nature* **531**, 489–493 (2016).
- Bourissou, D., Guerret, O., Gabbai, F. P. & Bertrand, G. Stable carbenes. *Chem. Rev.* **100**, 39–92 (2000).
- Hopkinson, M. N., Richter, C., Schedler, M. & Glorius, F. An overview of N-heterocyclic carbenes. *Nature* **510**, 485–496 (2014).
- Bellotti, P., Koy, M., Hopkinson, M. N. & Glorius, F. Recent advances in the chemistry and applications of N-heterocyclic carbenes. *Nat. Rev. Chem.* **5**, 711–725 (2021).
- Crudden, C. M. et al. Ultra stable self-assembled monolayers of N-heterocyclic carbenes on gold. *Nat. Chem.* **6**, 409–414 (2014).
- Zhukhovitskiy, A. V., MacLeod, M. J. & Johnson, J. A. Carbene ligands in surface chemistry: from stabilization of discrete elemental allotropes to modification of nanoscale and bulk substrates. *Chem. Rev.* **115**, 11503–11532 (2015).
- Crudden, C. M. et al. Simple direct formation of self-assembled N-heterocyclic carbene monolayers on gold and their application in biosensing. *Nat. Commun.* **7**, 12654 (2016).
- Wu, C.-Y. et al. High-spatial-resolution mapping of catalytic reactions on single particles. *Nature* **541**, 511–515 (2017).
- Smith, C. A. et al. N-Heterocyclic carbenes in materials chemistry. *Chem. Rev.* **119**, 4986–5056 (2019).
- Koy, M., Bellotti, P., Das, M. & Glorius, F. N-Heterocyclic carbenes as tunable ligands for catalytic metal surfaces. *Nat. Catal.* **4**, 352–363 (2021).
- Wang, G. et al. Ballbot-type motion of N-heterocyclic carbenes on gold surfaces. *Nat. Chem.* **9**, 152–156 (2017).
- Ranganath, K. V. S., Kloesges, J., Schaefer, A. H. & Glorius, F. Asymmetric nanocatalysis: N-heterocyclic carbenes as chiral modifiers of Fe₃O₄/Pd nanoparticles. *Angew. Chem. Int. Ed.* **49**, 7786–7789 (2010).
- Ernst, J. B. et al. Molecular adsorbates switch on heterogeneous catalysis: induction of reactivity by N-heterocyclic carbenes. *J. Am. Chem. Soc.* **139**, 9144–9147 (2017).
- Kaeffer, N., Liu, H.-J., Lo, H.-K., Fedorov, A. & Coperet, C. An N-heterocyclic carbene ligand promotes highly selective alkyne semihydrogenation with copper nanoparticles supported on passivated silica. *Chem. Sci.* **9**, 5366–5371 (2018).
- van Dongen, S. F. M., Elemans, J. A. A. W., Rowan, A. E. & Nolte, R. J. M. Processive catalysis. *Angew. Chem. Int. Ed.* **53**, 11420–11428 (2014).
- Inayah, A. et al. Self-assembly of N-heterocyclic carbenes on Au(111). *Nat. Commun.* **12**, 4034 (2021).
- Ren, J. et al. A unidirectional surface-anchored N-heterocyclic carbene rotor. *Nano Lett.* **20**, 5922–5928 (2020).
- Man, R. W. Y. et al. Ultrastable gold nanoparticles modified by bidentate N-heterocyclic carbene ligands. *J. Am. Chem. Soc.* **140**, 1576–1579 (2018).
- Mata, J. A., Poyatos, M. & Peris, E. Structural and catalytic properties of chelating bis- and tris-N-heterocyclic carbenes. *Coord. Chem. Rev.* **251**, 841–859 (2007).
- Cao, Z. et al. Chelating N-heterocyclic carbene ligands enable tuning of electrocatalytic CO₂ reduction to formate and carbon monoxide: surface organometallic chemistry. *Angew. Chem. Int. Ed.* **57**, 4981–4985 (2018).
- Clair, S. & de Oteyza, D. G. Controlling a chemical coupling reaction on a surface: tools and strategies for on-surface synthesis. *Chem. Rev.* **119**, 4717–4776 (2019).

28. Di Giovannantonio, M. et al. Insight into organometallic intermediate and its evolution to covalent bonding in surface-confined ullmann polymerization. *ACS Nano* **7**, 8190–8198 (2013).
29. Pawlak, R. et al. Bottom-up synthesis of nitrogen-doped porous graphene nanoribbons. *J. Am. Chem. Soc.* **142**, 12568–12573 (2020).
30. Eichhorn, J. et al. On-surface Ullmann coupling: the influence of kinetic reaction parameters on the morphology and quality of covalent networks. *ACS Nano* **8**, 7880–7889 (2014).
31. Fritton, M. et al. The role of kinetics versus thermodynamics in surface-assisted Ullmann coupling on gold and silver surfaces. *J. Am. Chem. Soc.* **141**, 4824–4832 (2019).
32. Simonov, K. A. et al. From graphene nanoribbons on Cu(111) to nanographene on Cu(110): critical role of substrate structure in the bottom-up fabrication strategy. *ACS Nano* **9**, 8997–9011 (2015).
33. Di Giovannantonio, M. et al. Mechanistic picture and kinetic analysis of surface-confined Ullmann polymerization. *J. Am. Chem. Soc.* **138**, 16696–16702 (2016).
34. Gross, L., Mohn, F., Moll, N., Liljeroth, P. & Meyer, G. The chemical structure of a molecule resolved by atomic force microscopy. *Science* **325**, 1110–1114 (2009).
35. Mönig, H. et al. Quantitative assessment of intermolecular interactions by atomic force microscopy imaging using copper oxide tips. *Nat. Nanotechnol.* **13**, 371–375 (2018).
36. Bakker, A. et al. Elucidating the binding modes of N-heterocyclic carbenes on a gold surface. *J. Am. Chem. Soc.* **140**, 11889–11892 (2018).
37. Kawai, S. et al. Direct quantitative measurement of the C=O center dot center dot H-C bond by atomic force microscopy. *Sci. Adv.* **3**, e1603258 (2017).
38. Ohmann, R. et al. Supramolecular rotor and translator at work: on-surface movement of single atoms. *ACS Nano* **9**, 8394–8400 (2015).
39. Schuler, B. et al. Adsorption geometry determination of single molecules by atomic force microscopy. *Phys. Rev. Lett.* **111**, 106103 (2013).
40. Huber, F. et al. Chemical bond formation showing a transition from physisorption to chemisorption. *Science* **366**, 235–238 (2019).
41. Ternes, M., Lutz, C. P., Hirjibehedin, C. F., Giessibl, F. J. & Heinrich, A. J. The force needed to move an atom on a surface. *Science* **319**, 1066–1069 (2008).
42. Meyer, J. et al. Tuning the formation of discrete coordination nanostructures. *Chem. Commun.* **51**, 12621–12624 (2015).
43. Robles, R. et al. Supramolecular chemistry based on 4-acetylbiphenyl on Au(111). *Phys. Chem. Chem. Phys.* **22**, 15208–15213 (2020).
44. Shi, Z. & Lin, N. Porphyrin-based two-dimensional coordination Kagome lattice self-assembled on a Au(111) surface. *J. Am. Chem. Soc.* **131**, 5376–5377 (2009).
45. Pan, Y. et al. Effect of lattice-gas atoms on the adsorption behaviour of thioether molecules. *Phys. Chem. Chem. Phys.* **14**, 10987–10993 (2012).
46. Yang, Z. et al. Orbital redistribution in molecular nanostructures mediated by metal–organic bonds. *ACS Nano* **8**, 10715–10722 (2014).
47. Jaklevic, R. C. & Elie, L. Scanning-tunneling-microscope observation of surface diffusion on an atomic scale: Au on Au(111). *Phys. Rev. Lett.* **60**, 120–123 (1988).
48. Liu, J. et al. Iodine-doping-induced electronic structure tuning of atomic cobalt for enhanced hydrogen evolution electrocatalysis. *ACS Nano* **15**, 18125–18134 (2021).
49. Eder, G. et al. Solution preparation of two-dimensional covalently linked networks by polymerization of 1,3,5-tri(4-iodophenyl) benzene on Au(111). *ACS Nano* **7**, 3014–3021 (2013).
50. Bieri, M. et al. Two-dimensional polymer formation on surfaces: insight into the roles of precursor mobility and reactivity. *J. Am. Chem. Soc.* **132**, 16669–16676 (2010).
51. Lipton-Duffin, J. A., Ivasenko, O., Perepichka, D. F. & Rosei, F. Synthesis of polyphenylene molecular wires by surface-confined polymerization. *Small* **5**, 592–597 (2009).
52. Li, H. K. et al. Nanoparticle PCR: nanogold-assisted PCR with enhanced specificity. *Angew. Chem. Int. Ed.* **44**, 5100–5103 (2005).
53. Franz, M. et al. Controlled growth of ordered monolayers of N-heterocyclic carbenes on silicon. *Nat. Chem.* **13**, 828–835 (2021).
54. Doud, E. A. et al. In situ formation of N-heterocyclic carbene-bound single-molecule junctions. *J. Am. Chem. Soc.* **140**, 8944–8949 (2018).
55. Zhang, H. et al. Surface supported gold-organic hybrids: on-surface synthesis and surface directed orientation. *Small* **10**, 1361–1368 (2014).
56. Amirjalayer, S., Bakker, A., Freitag, M., Glorius, F. & Fuchs, H. Cooperation of N-heterocyclic carbenes on a gold surface. *Angew. Chem. Int. Ed.* **59**, 21230–21235 (2020).
57. Linden, S. et al. Electronic structure of spatially aligned graphene nanoribbons on Au(788). *Phys. Rev. Lett.* **108**, 216801 (2012).
58. Bita, I. et al. Graphoepitaxy of self-assembled block copolymers on two-dimensional periodic patterned templates. *Science* **321**, 939–943 (2008).
59. Hapala, P., Temirov, R., Tautz, F. S. & Jelinek, P. Origin of high-resolution IETS-STM images of organic molecules with functionalized tips. *Phys. Rev. Lett.* **113**, 226101 (2014).

Publisher's note Springer Nature remains neutral with regard to jurisdictional claims in published maps and institutional affiliations.

Springer Nature or its licensor (e.g. a society or other partner) holds exclusive rights to this article under a publishing agreement with the author(s) or other rightsholder(s); author self-archiving of the accepted manuscript version of this article is solely governed by the terms of such publishing agreement and applicable law.

© The Author(s), under exclusive licence to Springer Nature Limited 2023

Methods

STM

An atomically clean crystal surface was prepared by several cycles of Ar⁺ sputtering and annealing. All the experiments were performed in an UHV low-temperature STM (LT-STM) system and non-contact atomic force microscopy systems operating at $T = 78$ K and 4.5 K. The molecules were deposited onto the clean surface and verified by LT-STM before growth. Both molecules were deposited on substrates held at room temperature (300 K).

nc-AFM

The nc-AFM measurements were performed under liquid helium in two low-temperature scanning probe systems from Scienta Omicron and Createc under UHV. For Scienta Omicron system using a CuOx tip, the used q-Plus sensor consists of an electrochemically etched tungsten tip mounted on a tuning fork with a resonance frequency of ~26 kHz. Its spring constant was about 2,000 N m⁻¹ and its quality factor Q was between 15,000 and 18,000. Measurements were acquired in constant-height mode with frequency modulation, where the oscillation amplitude was set to 1.0 Å. For the tip-functionalization-controlled tip indentations into oxide nano-domains of a partially oxidized Cu (110) (2 × 1) O surface were performed. The tip termination, symmetry and stability were directly confirmed by subsequent contrast analysis on the same surface as discussed in detail in previous works⁶⁰. After tip functionalization the sample was changed to the prepared Au(111) sample with the molecular structures of interest **IPrI₂**. For Createc system using CO-tip, all nc-AFM measurements were performed using a commercial qPlus tuning fork sensor in frequency modulation mode with a Pt/Ir tip. The resonance frequency is about 27.9 kHz, and stiffness about 1800 N m⁻¹.

XPS measurements

For every XPS measurement the sample surface was checked by scanning probe measurements. Both systems are connected via an in-situ sample transfer and have base pressures of -2×10^{-10} mbar. In the XPS chamber the sample is illuminated by a monochromated Al K α X-ray source. The excited photoelectrons from the sample are analysed by a SPECS PHOIBOS 100 hemispherical analyser using a 2D delayline detector.

nc-AFM simulation

The nc-AFM simulations were generated by a numerical model developed previously⁶¹. Specific mechanical and electro-static properties for the O-terminated Cu-tip (CO tip) were discussed in our previous work⁶⁰: the spring constants are 161.9 N m⁻¹ (1.7 N m⁻¹) for horizontal and 271.1 N m⁻¹ (326.9 N m⁻¹) for the vertical component. An oxygen atom was set as the probing particle and the effective charge of the tip is $-0.05e$. The optimized molecular structure and the corresponding Hartree potential are taken from DFT calculations as described below. Finally, the used numerical model generates the AFM contrast by calculating the frequency shift Δf in consideration of the tip parameters and the surface potential for a specific height.

Data availability

Data supporting the findings of this work are available within this paper or its Supplementary Information.

References

- Schulze Lammers, B. et al. Benchmarking atomically defined AFM tips for chemical-selective imaging. *Nanoscale* **13**, 13617–13623 (2021).
- Hapala, P. et al. Mechanism of high-resolution STM/AFM imaging with functionalized tips. *Phys. Rev. B* **90**, 085421 (2014).

Acknowledgements

F.G. and N.L.D. acknowledge financial support from the Deutsche Forschungsgemeinschaft (SFB 858 and SFB 1459), as do H.F. (SFB 858, FU 299/18-1) and H.M. (MO 2345/4-1, 519972808). Q.D. acknowledges financial support from the National Natural Science Foundation of China (U2032206) and the Strategic Priority Research Program of Chinese Academy of Sciences (XDB36000000). H.-J.G. acknowledges financial support from the National Natural Science Foundation of China (61888102) and the National Key Research and Development Program of China (2019YFA0308500). L.H. acknowledges financial support from the National Key Research and Development Program of China (2018YFA0305800). Computations were carried out using the PALMA II HPC cluster provided by the University of Münster.

Author contributions

F.G. and H.F. initiated the project. F.G., H.F., H.M., M.K. and J.R. designed the experiments and coordinated the study. M.K., A.N. and C.G. designed and synthesized the molecules. J.R. and B.S.L. performed the STM measurements and analysed them with H.M. and Q.D.; H.O., M.N. and N.L.D. performed DFT and ReaxFF calculations. B.S.L., H.M. and J.R. did the nc-AFM (CuOx-tips)/XPS experiments and interpreted the data. Q.Z., L.H., Y.X., J.R. and H.-J.G. did the nc-AFM experiment using CO-functionalized tips. J.R. wrote the manuscript together with M.K., H.O., Q.D., H.M., N.L.D., H.F. and F.G. All the authors read and commented on the manuscript.

Competing interests

The authors declare no competing interests.

Additional information

Supplementary information The online version contains supplementary material available at <https://doi.org/10.1038/s41557-023-01310-1>.

Correspondence and requests for materials should be addressed to Hong-Jun Gao, Harry Mönig, Nikos L. Doltsinis, Harald Fuchs or Frank Glorius.

Peer review information *Nature Chemistry* thanks Katharina Kaiser, Shigeki Kawai and the other, anonymous, reviewer(s) for their contribution to the peer review of this work.

Reprints and permissions information is available at www.nature.com/reprints.